Available online at www.sciencedirect.com
ScienceDirect
Journal of Crystal Growth 298 (2007) 394–398
JOURNAL OF CRYSTAL GROWTH
www.elsevier.com/locate/jcrysgro

Electronic band structures and transport properties of wurtzite indium nitride grown by metalorganic vapor phase epitaxy

W.Z. Shen[a,*], Z.W. Jia[a], J. Chen[a], H.B. Ye[a], H. Ogawa[b], Q.X. Guo[b]

[a]*Laboratory of Condensed Matter Spectroscopy and Opto-Electronic Physics, Department of Physics, Shanghai Jiao Tong University, 1954 Hua Shan Road, Shanghai 200030, PR China*

[b]*Department of Electrical and Electronic Engineering, Faculty of Science and Engineering, Saga University, Saga 840-8502, Japan*

Available online 20 November 2006

Abstract

We have carried out a detailed investigation on the electronic band structures and transport properties of a high-quality wurtzite indium nitride (InN) single crystal grown by metalorganic vapor phase epitaxy. With the aid of vacuum ultraviolet optical reflection spectrum in the range of 4.0–20.0 eV, together with the theoretical analysis, we were able to identify up to 8 electronic transitions, showing a clear picture for the critical point transitions in InN. The InN bulk and low mobility surface conduction have been extracted and found to be temperature (10–300 K) -independent in both electron concentration and mobility. We also revealed the effects of localization and electron–electron interactions in the low temperature (below 5 K) magnetoconductance of the degenerate semiconductor.

Keywords: A3. Metalorganic vapor phase epitaxy; B1. Nitrides; B2. Semiconducting indium compounds

1. Introduction

As a promising semiconductor among group III-nitride compounds, indium nitride (InN) has recently received intensive research interest. However, the growth of high-quality InN remains a formidable challenge due to the low dissociation temperature of InN and the extremely high equilibrium vapor pressure of nitrogen. Many of its fundamental optical properties are still not well known despite detailed investigations since the 1980s. In contrast to the recent extensive experimental studies of the fundamental energy bandgap, there are few references in the literature up to now concerning the high order electronic transitions in InN. Kasic et al. [1] employed spectroscopic ellipsometry to study the InN dielectric function up to 6.5 eV at room temperature. In combination with the theoretical band structures, they summarized the critical points of InN along with the literature data at ~4.8, 5.4, 5.6, and 6.1 eV, as well as the fundamental bandgap. On the other hand, band structures of InN have been widely studied by a number of theoretical models over the past 20 years, such as the *ab initio* calculations [2], and the empirical pseudopotential method (EPM) approach [3], to follow the experimental investigation, especially at the recent fundamental bandgap debate. The experimental study of the critical point transitions in InN will give a clear understanding of optical transition processes and electron band structures, which is not only of scientific interest, but also important for device applications.

In comparison with the detailed optical measurements, electrical measurements on InN are at their early stages. With the use of electron energy loss spectroscopy to probe the plasma excitations at different depths, Mahboob et al. [4] found a maximum electron density that occurs near the surface of InN epilayers, and it gradually declines to the bulk value, confirming the observation of surface charge accumulation by capacitance–voltage measurements. Swartz et al. [5] identified surface/interface and bulk conduction mechanisms in InN through the variable magnetic field Hall measurements. Inushima et al. [6] presented the temperature dependence of resistivity, magnetoresistance and Shubnikov–de Hass oscillations as a function of InN carrier density, while Thakur et al. [7]

*Corresponding author. Fax: +86 21 54743242.
E-mail address: wzshen@sjtu.edu.cn (W.Z. Shen).

0022-0248/$ - see front matter © 2006 Elsevier B.V. All rights reserved.
doi:10.1016/j.jcrysgro.2006.10.050

investigated the temperature dependence of Hall mobility and carrier concentration. Only n-type InN has been reported to date, except for the recent first evidence of successful p-type doping of InN by Jones et al. [8].

The motivations of the present paper are twofold. One is to present higher order critical point transitions by reporting reliable optical reflection in single crystal wurtzite InN thin films in the spectral range of 4.0–20.0 eV. We identified up to 8 electronic transitions with the aid of Adachi's dielectric function model [9] for the vacuum ultraviolet (VUV) reflection spectrum and the EPM approach [3] for the electronic band structures. The other is to examine the temperature dependence of the surface and bulk transport parameters (electron concentration and mobility) by the variable magnetic field Hall measurements, and reveal the effects of localization and electron–electron interactions in the magnetoconductance of the degenerate semiconductor.

2. Experimental details

The studied InN thin films were grown on (0 0 0 1) α-Al_2O_3 substrates by microwave-excited metalorganic vapor phase epitaxy (MOVPE) at temperature of 500 °C. Pure N_2 and trimethylindium were used as source materials. The trimethylindium was carried by pure N_2 gas into the chamber and then mixed into the N_2 plasma excited by 2.45 GHz microwave radiation. Reflection high-energy electron diffraction results [Fig. 1(a)] showed all the InN samples to be a single crystalline and to have an orientation relationship of (0 0 01) InN/(0 0 0 1) α-Al_2O_3. Only two diffraction peaks corresponding to the (0 0 0 2) and (0 0 0 4) reflections from InN were observed in the θ–2θ profiles [Fig. 1(b)], indicating that the c-axis of InN is perpendicular to the substrate surface. Raman spectrum [Fig. 1(c)] recorded in backscattering geometry of $z(x,-)\bar{z}$ configuration revealed sharp first-order Raman peaks of E_2 (low) at 89 cm^{-1}, E_2 (high) at 491 cm^{-1}, and A_1(LO) at 590 cm^{-1} phonon modes [10], with a full-width at half-maximum of the E_2 (high) peak ~8 cm^{-1}. The fact that we could not observe any Raman signal in the vicinity of the sharp N–N vibration in air at 2328 cm^{-1} indicated that there is no excess nitrogen in the present InN sample. The unintentionally doped InN films (thickness of 0.35 μm) exhibits n-type conductivity, with a Hall mobility of 365 $cm^2/V\,s$ and an electron concentration (n) of 2.8×10^{19} cm^{-3} at room temperature.

Raman spectra were taken with an Ar^+ laser (514.5 nm) under a Jobin Yvon LabRAM HR 800 micro-Raman system with an Andor DU420 classic CCD detector. VUV reflection spectra were measured between 4 and 20 eV at the beam line of the SOR-RING in the Institute for Solid State Physics of the University of Tokyo with a 1-m Seya-Namioka type monochromator. Synchrotron radiation photoemission spectroscopy was carried out using the radiation from the 750 MeV electron storage ring of UVSOR at the Institute for Molecular Science. The magnetic field dependent Hall and conductivity measurements were performed in the Van der Pauw configuration by a set of Keithley Hall measurement system, including a

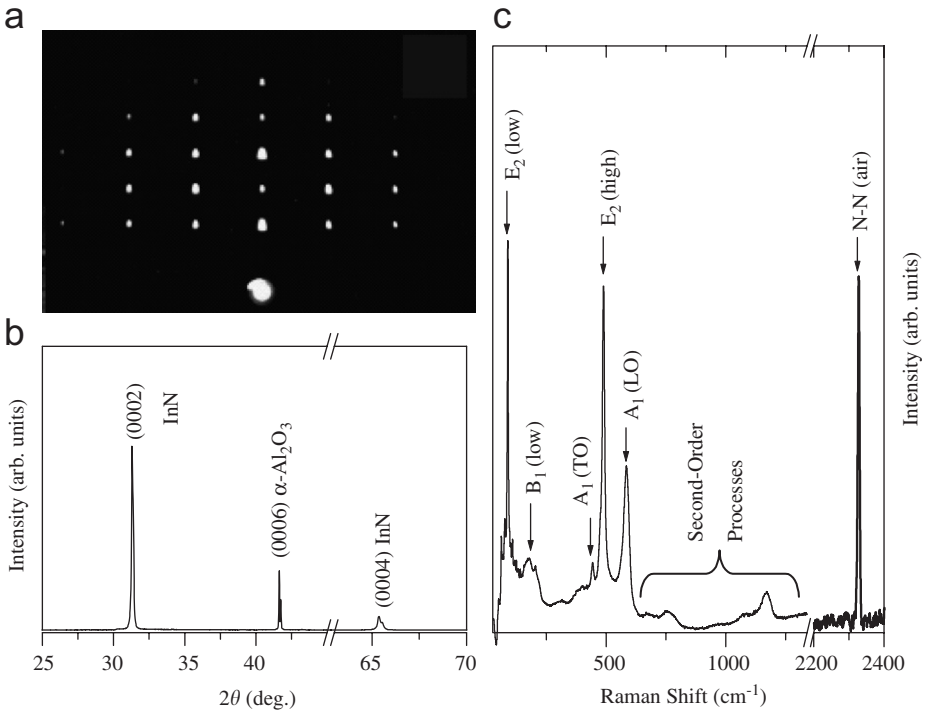

Fig. 1. (a) Reflection high-energy electron diffraction pattern, (b) X-ray diffraction, and (c) Raman scattering of a typical wurtzite InN thin film grown by MOVPE.

220 programmable current source, 2182 nanovoltmeter, and 7001 switch system with a 7065 Hall card. The Ohmic contacts were fabricated by alloying indium on the surface of the InN thin films. The samples were immersed in a ^{4}He cryostat system equipped with a 15 T Oxford Instruments superconductive magnet, where the measured temperature can come down to 1.4 K. The magnetic field reading accuracy was better than 1%.

3. Results and discussion

Fig. 2(a) displays the room-temperature synchrotron reflection spectrum of the InN in the range of 4.0–20.0 eV. The solid squares are the experimental data, while the solid curve is the calculated spectrum employing Adachi's dielectric function model [9], showing a fairly good agreement with the experimental data. Through the calculation, taking into account the contributions of the lowest-direct gap and E_1 transitions with their excitonic transitions, higher-lying critical point transitions, and the additive constant due to the transitions beyond the spectral range, we can observe 7 clear transition structures (marked from A to G) in the VUV reflection spectrum. After self-correction of a 'scissors operator' (constant shift) of 0.45 eV, the EPM electronic band structures of InN by Fritsch et al. [3] yield a complete and reliable band dispersion of valence and conduction bands, and the critical points in the EPM band structures can describe quite well all the major structures in our reflection spectrum. The theoretical band structures of AlN by the same research group have also been explained well by our experimental critical point transitions in wurtzite AlN [11].

The structure A can be assigned to the E_1 critical point transition, which usually occurs at the saddle point inside the zone of the (1 1 1) direction (U point). Through calculation, two fitting peaks with the photon energies around 4.90 and 5.43 eV are involved in the broad structure, and have been assigned to the transitions of U_{4v}–U_{3c} and U_{3v}–U_{3c}, respectively. From the viewpoint of dielectric function models, high-lying transitions are characterized with a certain number of damped harmonic oscillators and the calculated oscillator energies represent the center positions of the structures in the reflection curve. Structure B appears to be a shoulder around 6.2 eV. More than one critical point transitions are possibly involved within that energy region, since, in principle, all of the allowed critical point transitions from the valence band to the conduction band can take place simultaneously and be recorded in the reflection spectrum. Here, we list two main critical point transitions H_{3v}–H_{3c} (6.19 eV) and/or M_{3v}–M_{1c} (6.27 eV), which may contribute to the structure B.

By comparing our experimental data with the EPM results for each of the main critical point transitions, we also identified the higher-lying structures of C to G, as listed in Fig. 2(a). The calculated structure positions at room temperature are 7.80, 8.80, 9.90, and 10.95 eV for peaks C to F, which correspond well with the transitions of K_{3v}–K_{2c} (7.98 eV), A_{56v}–A_{13c} (8.87 eV), H_{3v}–H_{12c} (9.84 eV), and Δ_{1v}–Δ_{6c} (10.92 eV), respectively, in the EPM band structures after the 'scissors operator' correction. The structure G may be attributed to the higher-lying critical point transitions, such as L_{13v}–L_{13c} (12.82 eV) and/or A_{13v}–A_{13c} (12.98 eV), with the calculated photon energy of about 12.8 eV.

Fig. 2(b) presents the photoelectron spectrum of the InN, excited with a synchrotron radiation at a photon energy of 40 eV. As we know, photoelectron energy distribution is directly related to the density of states in the valence band, and can be used to probe the electronic density of states and test the validity of the existing theoretical band structures of InN. In addition to the observation of In4d and N2s states at the binding energies of 15.9 and 11.4 eV, respectively, a valence band width of ~10 eV can be estimated for the hexagonal InN with two distinguishable features at 3.9 and 7.4 eV. Reasonable agreement for the valence band width has also been found

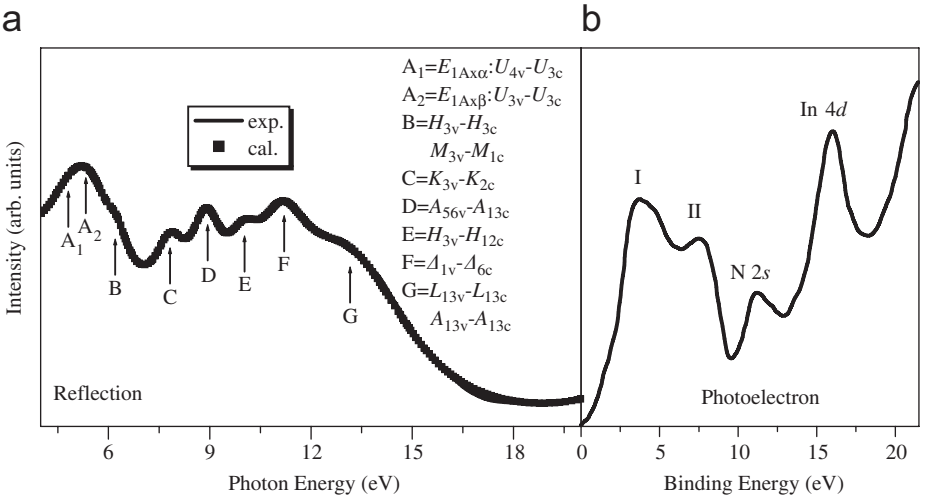

Fig. 2. Room-temperature synchrotron radiation (a) VUV reflection, and (b) photoelectron spectra of the wurtzite InN thin film grown by MOVPE.

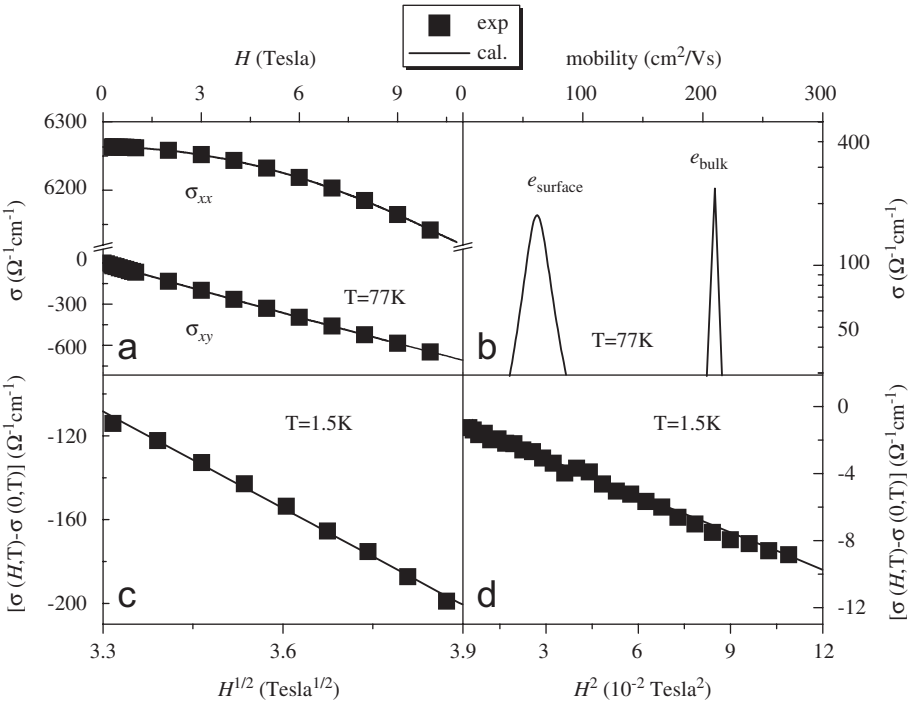

Fig. 3. (a) Magnetic-field-dependent conductivity tensors, (b) corresponding mobility spectrum, and magnetoconductance at (c) high and (d) low magnetic fields of the MOVPE InN.

between our experimental data and that calculated under EPM.

Now, we move to the transport properties of the MOVPE InN thin film. Fig. 3(a) shows the magnetic field (H) dependence of the experimental results (solid squares) at 77 K, in the form of conductivity components $\sigma_{xx}(H)$ and $\sigma_{xy}(H)$. The experimental fact that we observed negative values of $\sigma_{xy}(H)$ throughout the magnetic field reflects the n-type nature of the measured InN sample. It should be noted that traditional fixed magnetic field Hall measurements only give average carrier concentration and mobility. In combination with mobility spectra analysis (MSA) procedures [12], the variable magnetic field Hall measurements can yield the distribution of electron mobility and extract the transport parameters of all carrier species present within the sample that contributes to the conducting processes. The MSA would transform the experimental magnetic field-dependent Hall data into the dependence of the conductivity concentration function on the mobility, in which each kind of carrier contributing to the total conductivity appears as a separate peak at a given mobility. Fig. 3(b) displays the corresponding mobility spectrum obtained via the MSA procedures, where we clearly identified the InN bulk and low mobility surface conduction. The solid curves in Fig. 3(a) are the calculated $\sigma_{xx}(H)$ and $\sigma_{xy}(H)$ obtained using the carrier concentrations and mobility distributions in Fig. 3(b), which show good agreement with the experimental data.

It is found that the InN sample shows temperature (10–300 K) independent characteristics in electron concentration and mobility for both the bulk and surface carriers. The underlying physical origin is as follows. On the one hand, the donors are fully ionized in high carrier density semiconductors, and the carrier concentration approximately equals the donor concentration, which is independent of temperature. The theoretical calculation of carrier concentration, taking into account the donors, acceptors, thermal activation energy, etc., yields good agreement with the experimental data under an activation energy of ~0.1 eV, which is so large that the thermally activated concentration is negligible below room temperature. On the other hand, the scattering rates can be calculated using Born-scattering theory at the Fermi energy, since electron scattering is mainly confined to the Fermi surface in strongly degenerate semiconductors. We found that, in the high carrier density InN thin film, the dominant charged center scattering at low temperatures has very weak temperature dependence, while the electron-longitudinal optical phonon scattering increases steadily at high temperatures, i.e., almost temperature independent of the total mobility over the whole measured temperature range. In contrast, the mobility will first experience increase and then decrease with the increase of temperature in low carrier density semiconductors.

The dependence of resistance on temperature and magnetic field in the studied InN sample is typical for a semiconductor in the metallic side of metal–insulator transition, except for the very low temperatures of below 5 K, where rapid increase of the conductivity has been observed with decreasing temperature due to the weak localization effects. Nevertheless, localization and electron–electron interactions both play important roles in

determining the behavior of the electronic transport. The contribution to the magnetoconductance due to electron–electron interactions is negative and arises predominantly from the Zeeman splitting of the spin-up and spin-down bands. The magnetoconductance due to the weak localization involves interplay of the magnetic field, inelastic-scattering, spin–scattering, and spin-orbit processes. The weak localization also gives negative magnetoconductance in InN films, since InN is supposed to have strong spin–orbit effects [6]. Both the localization and electron–electron interactions have the same limiting behavior for magnetoconductance, namely, proportional to H^2 at very low and to $H^{1/2}$ at very high magnetic fields. According to the localization-interaction model [13] for degenerate semiconductors in the metallic side of the Mott transition, the electron–electron interactions dominate the magnetoconductance at very low temperatures and high magnetic fields with the behavior proportional to $H^{1/2}$ [Fig. 3(c)]. Detailed separation for the weak localization contribution from the component due to the interactions [Fig. 3(d), both proportional to H^2 at low magnetic fields] yields an inelastic-scattering length of 180 nm (or time of 1.35×10^{-10} s) for the InN at 1.5 K.

4. Conclusions

In summary, by the aid of Adachi's dielectric function model and the EPM approach, we presented a clear picture for the electronic band structures in wurtzite InN by identifying up to 8 electronic transitions in the VUV reflection spectrum over the wide range from 4.0 to 20.0 eV. We separated the InN bulk and low mobility surface conduction by the variable magnetic field Hall measurements, where both electron concentration and mobility are found to be temperature (10–300 K) independent. The analysis of low temperature (below 5 K) magnetoconductance of the degenerate semiconductor demonstrates the effects of localization and electron–electron interactions, yielding an inelastic-scattering length of 180 nm for the InN at 1.5 K.

Acknowledgments

This work was supported by the Natural Science Foundation of China under contract Nos. 10125416, 60576067, and 10674094 the National Minister of Education Program for Changjiang Scholars and Innovative Research Team in University (PCSIRT), the Grant-in-Aid for Scientific Research (c) (No.16560013) from the Ministry of Education, Culture, Sports, Science, and Technology, Japan, and the Venture Business Laboratory of Saga University.

References

[1] A. Kasic, E. Valcheva, B. Monemar, H. Lu, W.J. Schaff, Phys. Rev. B 70 (2004) 115217.
[2] F. Bechstedt, J. Furthmüller, J. Crystal Growth 246 (2002) 315.
[3] D. Fritsch, H. Schmidt, M. Grundmann, Phys. Rev. B 69 (2004) 165204.
[4] I. Mahboob, T.D. Veal, C.F. McConville, H. Lu, W.J. Schaff, Phys. Rev. Lett. 92 (2004) 036804.
[5] C.H. Swartz, R.P. Tompkins, N.C. Giles, T.H. Myers, H. Lu, W.J. Schaff, L.F. Eastman, J. Crystal Growth 269 (2004) 29.
[6] T. Inushima, M. Higashiwaki, T. Matsui, T. Takenobu, M. Motokawa, Phys. Rev. B 72 (2005) 085210.
[7] J.S. Thakur, R. Naik, V.M. Naik, D. Haddad, G.W. Auner, H. Lu, W.J. Schaff, J. Appl. Phys. 99 (2006) 023504.
[8] R.E. Jones, K.M. Yu, S.X. Li, W. Walukiewicz, J.W. Ager, E.E. Haller, H. Lu, W.J. Schaff, Phys. Rev. Lett. 96 (2006) 125505.
[9] S. Adachi, J. Appl. Phys. 68 (1990) 1192.
[10] Z.G. Qian, W.Z. Shen, H. Ogawa, Q.X. Guo, J. Phys.: Condens. Matter 16 (2004) R381.
[11] J. Chen, W.Z. Shen, H. Ogawa, Q.X. Guo, Appl. Phys. Lett. 84 (2004) 4866.
[12] W.A. Beck, J.R. Anderson, J. Appl. Phys. 62 (1987) 541.
[13] P.A. Lee, T.V. Ramakrishnan, Rev. Mod. Phys. 57 (1985) 287.